JOURNAL OF AIRCRAFT
Vol. 60, No. 4, July–August 2023

Finite Element Simulation of Three Full-Scale Crash Tests for Cessna 172 Aircraft

Brian H. Mason* and Jerry E. Warren, Jr.†
NASA Langley Research Center, Hampton, Virginia 23681-2199

https://doi.org/10.2514/1.C037125

The NASA Emergency Locator Transmitter Survivability and Reliability project was initiated in 2013 to assess the crash performance standards for the next generation of emergency locator transmitter (ELT) systems. Three Cessna 172 aircraft were acquired to perform crash testing at the NASA Langley Research Center Landing and Impact Research Facility. Full-scale crash tests were conducted in the summer of 2015, and each test article was subjected to severe, but survivable, impact conditions including a flare-to-stall during emergency landing and two controlled-flight-into-terrain scenarios. Finite element analyses were performed to numerically simulate the aircraft response to the crash tests. The first test simulated impacting a concrete surface represented analytically by a rigid plane. Tests 2 and 3 simulated impacting a dirt surface represented analytically by an Eulerian grid of brick elements using a Mohr–Coulomb material model. The objective of this paper is to summarize the test and analysis results for the three full-scale crash tests. Simulation models of the airframe that correlate well with the tests are needed for future studies of alternate ELT mounting configurations.

I. Introduction

A. Motivation and Background

IN 2013, the NASA Search and Rescue (SAR) Mission Office at NASA Goddard Space Flight Center initiated a study to assess the crash performance standards of the next generation of emergency locator transmitters (ELTs). SAR is particularly interested in ensuring that ELTs are not mounted in locations in which ELTs or their wired antenna connections will be damaged during a crash. In pursuit of this ELT-SAR study, three Cessna 172 aircraft were acquired by NASA and subjected to severe but survivable crash tests in the summer of 2015. The crash tests enabled evaluation of ELT performance under conditions that more accurately replicated actual crash environments than those found in the current performance standard [1]. Each aircraft was equipped with four to five ELTs. These crash tests were conducted at the Landing and Impact Research Facility (hereafter referred to as LandIR) [2,3] at NASA Langley Research Center (hereafter referred to as LaRC). A photograph of the LandIR is shown in Fig. 1. The details of the test setup and rigging are documented in another publication [4]. The data from the three tests were used to calibrate structural finite element (FE) models of the airframes. Once calibrated, these models can be used to predict the airframe and ELT responses at various aircraft impact conditions. The analyses will lead to updated installation standards for the entire ELT system (beacon, antenna, and interconnecting cabling).

Beginning in the mid-1970s, the LandIR facility at LaRC was used for testing general aviation (GA) aircraft for improved crashworthiness [5–13]. Data from tests conducted between 1974 and 1983 were used to assist the Federal Aviation Administration in establishing seat certification standards [14]. The Advanced General Aviation Transport Experiments (AGATE) program was established in the late 1990s as a collaboration between government and industry to revive the GA market. Full-scale crash tests of a Beech Starship in 1995 and a modified Lancair aircraft in 2001 were performed as technology demonstrations for AGATE [15,16]. The LandIR is a unique facility [17] that is well suited for performing the general aviation aircraft crash tests planned by the ELT-SAR project.

The Cessna 172 Skyhawk is a four-seat single-engine high-wing airplane manufactured by the Cessna Aircraft Company. More Cessna 172s have been built than any other aircraft, and the first production models were delivered in 1956. These aircraft were selected for this series of crash tests for their availability and because ELT installation and setup do not vary significantly in aluminum alloy general aviation airframes. It is also noted that NASA had previously conducted a series of crash tests using C-172 aircraft in the 1970s [9,18], and these tests helped guide the development of the lifting hardware used in the current tests.

B. Objective

The purpose of this paper is to correlate explicit dynamic FE simulation models with data from the experimental tests. Correlation of the models includes comparison of the airframe weight, center of gravity, kinematic response, delta velocity (or rebound velocity), and accelerometer data between the simulation model and the experimental tests. Simulation models that represent the kinematic response of the airframe well can then be used to evaluate alternative ELT mounting configurations. Additionally, this work serves as an example for simulation of ground impact landings for other classes of aircraft, including transport-category aircraft [19,20] as well as newer urban air mobility class vehicles.

C. Test Description

The three Cessna high-wing four-seat GA airplanes used for this test series are shown in Fig. 2. Test article 1 was a 1958 C-172. Test article 2 was a 1958 C-175, which was built on the C-172 airframe but contains a different engine and gearbox. The third test article was a 1975 C-172M. Test articles 1 and 3 were operational until the winter of 2014 before their purchase by LaRC.

Each aircraft was outfitted with similar instrumentation, cameras, and onboard experiments. Although only one ELT is required in a GA aircraft, for testing purposes, multiple ELTs were mounted into the cabin or tail section of each aircraft for the evaluation of their performance. The rear seats and luggage area equipment were removed from each airplane, and an onboard data acquisition system (DAS) was installed in their place. The DAS recorded accelerations throughout the fuselage at a sampling rate of 10 kHz. A frame assembly was constructed on the top of the wing for rigging the airframe to the LandIR. Further information about the instrumentation and rigging hardware for the tests was presented in a paper by Littel [4].

Presented as Paper 2017-0631 at the 2017 AIAA Science and Technology (SciTech) Forum and Exposition, Grapevine, TX, January 9–13, 2017; received 25 July 2022; revision received 11 January 2023; accepted for publication 25 March 2023; published online Open Access 6 June 2023.

*Research Aerospace Engineer, Structural Mechanics and Concepts Branch, Mail Stop 190. Associate Fellow AIAA.

†Research Aerospace Engineer, Structural and Thermal Systems Branch, Mail Stop 431. Member AIAA.

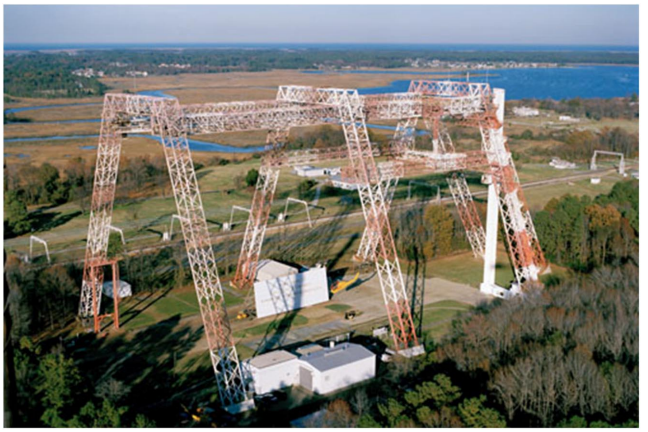

Fig. 1 NASA Landing and Impact Research facility.

All tests were conducted within the approximate landing stall speed of the aircraft. Test 1 was designed to simulate a flare to touchdown onto a rigid surface (concrete). This case provided a way to isolate the airframe response for model calibration. Tests 2 and 3 were designed to simulate controlled-flight-into-terrain conditions, where the terrain response must also be accounted for in the models. Test 2 featured the airplane impacting with a nosedown attitude, whereas test 3 featured the airplane impact with a noseup attitude resulting in tail strike. Tests 2 and 3 impacted a dirt surface consisting of a clay–sand mixture known as gantry unwashed sand (GUS) [21]. This soil was used as the impact surface for the transport rotorcraft airframe crash testbed full-scale tests [22]. Preliminary analytical results for the three crash tests were previously presented [23]. Analytical results from LS-DYNA simulations were previously reported for crash tests 1 [24] and 2 [25]. The as-measured impact conditions are presented in Table 1, where the horizontal and vertical directions are defined as normal and parallel to the ground, respectively.

II. Model Geometry and Loads

In this section, the computer models used to simulate the impact tests are described. The derivation of the geometry for the models is described first. Next, material properties for the model are discussed. In the third part of this section, the FE model mesh representation is described.

A. Geometry for Analytical Models

Development of the FE models was complicated by the fact that no prior geometry or static load models of the C-172 airframe existed and no engineering drawings were available. Consequently, an original computer-aided design geometry of the airframe was generated using both a three-dimensional laser scan and hand measurements of the test article. The measurements were used as inputs to the Conceptual Design Shop (CDS) tool [26]: an airframe geometry generation tool developed within the PATRAN FE modeling software [27]. The initial geometry from the CDS was tuned to match the point cloud from the laser scan, as shown in Fig. 3. The CDS-generated geometry included the internal structure (ribs, spars, frames, etc.) of the airframe. The FE model was discretized from this geometry, although several additional structural components (ELTs, point masses, and LandIR mounts) were added later.

Simulations for the test 1 and 2 configurations used the same C-172 FE airframe model. For the test 3 C-172M airframe, the fuselage aft of frame 108 was replaced with the swept tail geometry with a rear window and a narrower aft fuselage section, as shown in Fig. 4.

Table 1 Crash conditions at impact

Test	Surface	Vertical velocity, in./s (ft/min)	Horizontal velocity, in./s (kt)	Pitch angle, deg	Pitch rate, deg/s
1	Concrete	276.0 (1380)	722.4 (35.7)	+1.48	+16.5
2	GUS	344.4 (1722)	823.2 (40.6)	−12.20	+16.1
3	GUS	283.2 (1416)	682.8 (33.7)	+8.0	+13.1

B. Material Properties

Due to the lack of data from the manufacturer, the exact material properties and component dimensions (thicknesses, beam heights, rod diameters, etc.) were unknown. Because of the large number of components in the aircraft, extensive strength and stiffness testing of all components in the aircraft was not practical, and so material properties commonly used in aircraft were assumed as shown in Table 2. A magnet was used to determine that the engine mounts, landing gear, and firewall contained ferric steel; all other metallic components were assumed to be constructed of aluminum alloys. The engine and DAS boxes were not modeled in detail, but their average

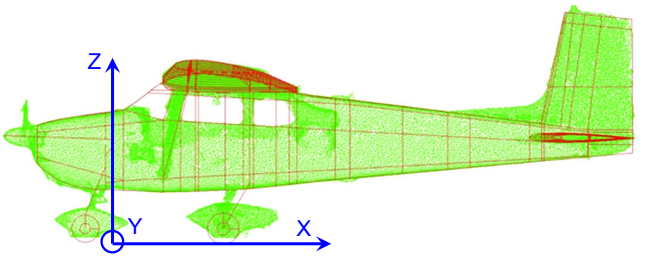

Fig. 3 CDS geometry (red) and laser scanned data (green) for C-172 airframe.

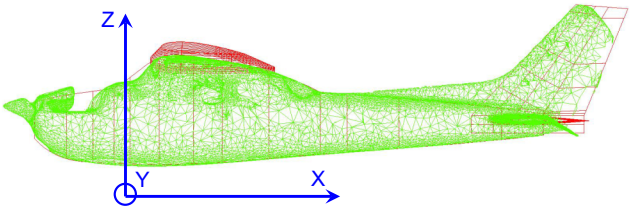

Fig. 4 CDS geometry (red) and laser scanned data (green) for C-172M airframe.

Fig. 2 ELT-SAR crash test articles.

Table 2 Material elastic properties[a]

Material	Elastic modulus, Msi	Poisson's ratio ν	Mass density, lb · $fs^2/in.^4$	Yield stress, ksi
Steel	30.0	0.300	7.359×10^{-4}	90.0
Aluminum	10.0	0.300	2.525×10^{-4}	40.0
Rubber	0.357	0.323	2.588×10^{-4}	15.0
Glass	0.500	0.300	1.124×10^{-4}	n/a

[a]n/a denotes "not applicable."

densities were tuned to match the measured weight. A series of hand measurements was taken of the panel thicknesses at key locations in the aircraft (forward fuselage, aft fuselage, rib, spar, wing covers, etc.). The shock absorber in the nose landing gear is represented by a slot connector element using the load displacement curve shown in Fig. 5. The shock absorber properties in Fig. 5 were derived from measurements of the test aircraft. The first point in Fig. 5 represents the shock absorber displacement under aircraft weight. For the second point, the shock absorber is assumed to be fully compressed when 1.9 times the gross takeoff weight (GTOW) of the aircraft is supported entirely by the nose wheel.

The final tuning of the mass of the computer models to the actual aircraft was accomplished through the use of point masses. For test 1, four point masses (totaling 220 lbf) were added to the model to match the weight and center of gravity (CG) of the test article, as shown in Table 3. The global coordinate system for the model is shown in Fig. 3. The test 2 configuration is heavier than test 1, and two point masses (totaling 321 lbf) were added to the model to match the weight and CG of the test article, as shown in Table 4. For test 3, four point

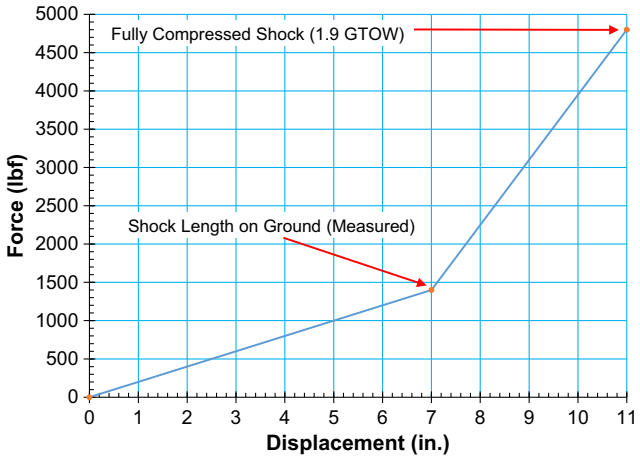

Fig. 5 Derived load–displacement curve for nose landing gear shock.

Table 3 Test and analysis values of inertial properties for test 1

Parameter	Test	Model	Difference	Difference, %
Weight, lbf	2000.000	2000.013	0.013	0.001
CG_x, in.	44.500	44.500	0.000	0.000
CG_y, in.	0.000	−0.028	−0.028	n/a
CG_z, in.	46.250	46.428	0.178	0.385

Table 4 Test and analysis values of inertial properties for test 2

Parameter	Test	Model	Difference	Difference, %
Weight, lbf	2114.000	2113.986	−0.014	−0.001
CG_x, in.	39.500	39.500	0.000	0.000
CG_y, in.	0.000	−0.088	−0.088	n/a
CG_z, in.	48.100	48.100	0.000	0.00

Table 5 Test and analysis values of inertial properties for test 3

Parameter	Test	Model	Difference	Difference, %
Weight, lbf	2072.000	2071.980	−0.020	−0.001
CG_x, in.	42.500	42.500	0.000	0.001
CG_y, in.	0.000	0.073	0.073	n/a
CG_z, in.	50.800	50.601	−0.199	−0.392

masses (totaling 393 lbf) were added to the model to match the weight and CG of the test article, as shown in Table 5.

C. Analysis Models

All FE analyses are performed with Abaqus software, which is a product of Simulia [28]. The Abaqus model representing the test 1 configuration is shown in Fig. 6. A nominal shell element edge length of 1.5 in. was used. This model contains 71,514 nodes, 235 beam elements, 74,640 shell elements, 400 solid elements, 66 multipoint constraints, four different materials, four revolute connectors (wheel axles), and 22 concentrated masses. The concrete impact surface was modeled as a horizontal rigid shell element, and the aircraft was set at an initial position of 0.1 in. above that surface. All shell elements were defined as Abaqus S3R and S4R elements (three- and four-noded reduced order shells, respectively), and the beam elements were defined with Abaqus B31 (three-dimensional linear beam) elements. The four ELTs, the DAS box, and the tires were modeled as C3D8 (three-dimensional eight-noded continuum) solid elements. The engine, seats, dummy occupants, and fuel in the wing were simulated as concentrated masses. The model required 4.5 h of wall-clock time on an eight-processor Windows 7 workstation using Abaqus/Explicit version 6.14 to simulate 0.30 s of impact.

The Abaqus model representing the test 2 configuration is identical to the test 1 configuration, with the following exceptions. First, the number and position of the ELTs (five instead of four) are different. Second, the nose landing gear shock in the test article was damaged and locked in place; so, the spring shock used to represent the landing gear in test 1 is replaced with a 1-in.-long rigid beam. This beam is set up to break when the bending moment exceeds 240,000 lbf·in. to simulate the failure of the nose gear observed during the test. And finally, the impact surface in test 2 is soil (30 in. deep), which is modeled in Abaqus with an Eulerian grid of 63,000 eight-node brick elements measuring 4 in. long by 3 in. wide by 2.5 in. deep. Soil properties are represented with the Mohr–Coulomb plasticity model [28] with a density of 1.86×10^{-4} lbf · $s^2/in.^4$ and a friction angle of 30 deg. The model required 20 h of wall-clock time on an eight-processor Windows 7 workstation using Abaqus/Explicit version 6.14 to simulate 0.30 s of impact, which is noticeably higher than the test 1 runtime due to the additional soil elements and contact with the soil.

The Abaqus model representing the test 3 configuration is shown in Fig. 7. A nominal shell element edge length of 1.5 in. was used. This model contains 68,133 nodes, 331 beam elements, 69,064 shell elements, 976 solid elements, 42 multipoint constraints, eight materials, four revolute connectors (wheel axles), and 24 concentrated masses. The major components (wing, fuselage, empennage, landing gear, etc.) are represented with the same types of elements as described for test 1.

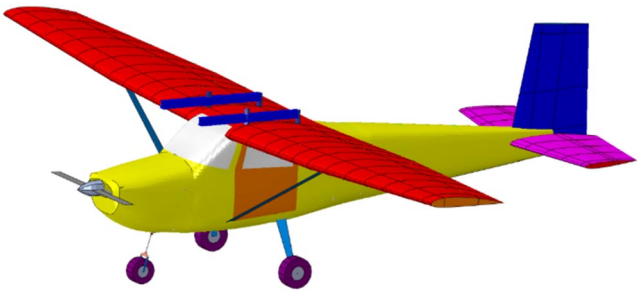

Fig. 6 Abaqus model of C-172 airframe (tests 1 and 2).

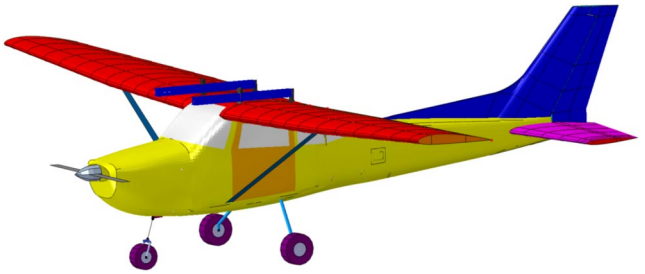

Fig. 7 Abaqus model of C-172M airframe (test 3).

The impact surface in test 3 is soil (30 in. deep), which is modeled in Abaqus with 95,040 eight-node brick elements measuring 4 in. long by 3 in. wide by 2.5 in. deep and uses the same properties as given for test 2. Rigid pins connecting the forward and aft fuselages are set up to break when the tensile reaction forces exceed 1000 lbf. For all analyses, the nodal location–, velocity–, and acceleration–time histories at the accelerometer locations were extracted from the results file.

III. Test and Analysis Correlation

In this section, the results of the FE simulations of crash tests 1, 2, and 3 are presented and compared with experimental data. All three numerical models were calibrated after the experimental tests. The calibration process included minor improvements to the modeling of the landing gear due to mass and stiffness uncertainties. Initial conditions for the numerical models (test article velocities, pitch angle, and pitch rate) were matched to the observed test values, as provided in Table 1.

A. Crash Test 1

A sequence of photographs taken from a high-speed camera is shown in Fig. 8, along with corresponding views of the matching model kinematics. Overall, the simulation matches the gross kinematics of the test well; the difference in the tail impact was only about 0.01 s. The pitch angle from photogrammetry during the test and simulation is plotted against time in Fig. 9. Simulation data were collected at the accelerometers, and the closest accelerometer to the CG (where photogrammetry data were collected) is installed on the pilot floor.

Comparisons of the test and analysis results of the rebound velocity (difference between impact velocity and minimum velocity, also called delta velocity), average acceleration, and peak acceleration in the vertical Z direction at several locations in the airframe are presented in Table 6. Only vertical accelerations are presented because the horizontal accelerations were low. Comparisons in the vertical Z direction are presented for three selected locations in the airframe (left door frame, DAS box, and rear bulkhead) in Fig. 10. Test and analytical acceleration data are filtered using an SAE channel filter class (CFC) 20 low-pass filter [29]. Acceleration data are presented in the local reference frame (moves with aircraft, as shown in Fig. 3) of each accelerometer. Velocities are presented in the global coordinate system (shown in Fig. 8). Analytical accelerations and velocities are computed in the fixed global coordinate system. For comparison with the test data, the analytical accelerations are translated into the moving local coordinate system. The photogrammetry data used to compute the pitch angles in Fig. 9 are used to transform the accelerometer data into the fixed coordinate system; these transformed accelerations are integrated to produce velocity–time histories for the test.

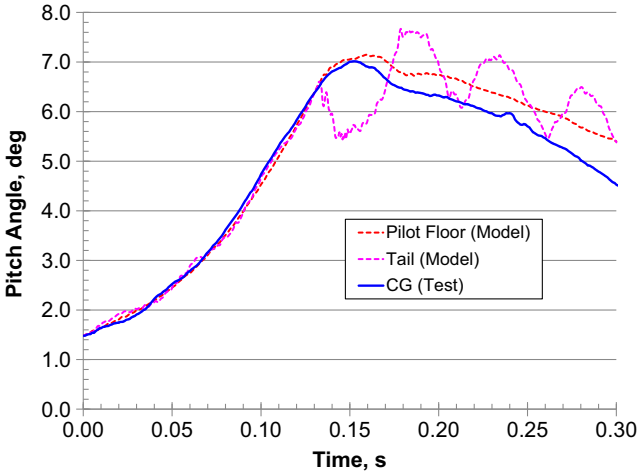

Fig. 9 Pitch angle from test and simulation against time for two locations in test 1.

Test and analysis comparisons of the delta velocity and average accelerations in the airframe are excellent; but, comparisons are generally poor for the peak accelerations. Contributors to the difference in the test and simulated accelerations include uncertainties in the timing of events and the analytically perfectly rigid impact surface. Peak accelerations are also significantly affected by uncertainties in component thicknesses and weight distributions (which could not be easily measured) and lack of detail in modeling components in the vicinity of the accelerometers (such as the DAS box, the unmodeled seats, and unmodeled anthropomorphic test dummies).

B. Crash Test 2

A sequence of photographs taken from the high-speed camera is shown in Fig. 11, along with corresponding views of the matching model kinematics. Note that the simulation model is cut in half (along the XZ-symmetry plane) to show the internal structure and the nose gear soil penetration. The pitch angle from photogrammetry during the test and simulation is plotted against time in Fig. 12. The simulation predicts a nosedown rotation of the aircraft at 0.03 s after impact, which is about 0.10 s earlier than the rotation occurs in the test. Buckling of the aft tail section also occurs significantly earlier in the simulation than in the test; however, the rate of bending of the aft tail section after initiation of buckling is similar. In the test, the airframe maintains an almost constant pitch angle for 0.12 s after impact, suggesting that the modeled soil may be too stiff and is causing the nose gear of the model to dig in and flip the aircraft sooner than in the test.

In Table 7, test and analysis comparisons of the delta velocity, average acceleration, and peak acceleration for the horizontal X and

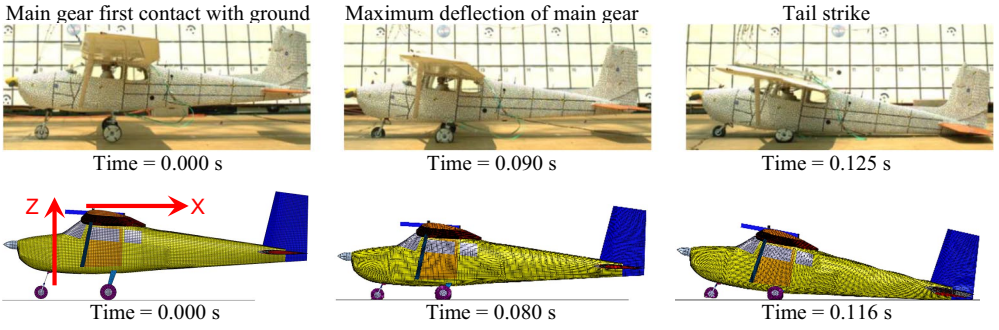

Fig. 8 Photographic images and computational results at critical kinematic events for test 1.

Table 6 Comparison of test and analysis of vertical velocity and acceleration at several locations for test 1

	Average acceleration, *g*			Peak acceleration, *g*			Delta velocity, in./s		
	Test	Model	Difference, %	Test	Model	Difference, %	Test	Model	Difference, %
Pilot Z	3.5	3.9	11.5	7.6	11.4	50.1	398.0	394.6	−0.9
Copilot Z	3.7	3.8	2.4	7.2	10.5	44.4	388.5	394.1	1.4
Left door Z	3.8	4.0	4.9	10.4	13.3	27.4	401.7	410.1	2.1
Right door Z	3.8	4.0	7.6	10.8	12.7	17.4	426.3	407.9	−4.3
DAS Z	4.2	4.0	−2.6	12.9	16.4	27.4	440.5	429.2	−2.6
Rear bulkhead Z	4.8	5.4	12.1	37.2	51.7	38.7	514.5	503.2	−2.2
Ceiling Z	3.8	4.0	4.8	9.8	17.8	81.3	414.0	416.6	0.6
Firewall Z	3.9	4.1	4.6	8.7	8.4	−3.8	377.0	373.9	−0.8

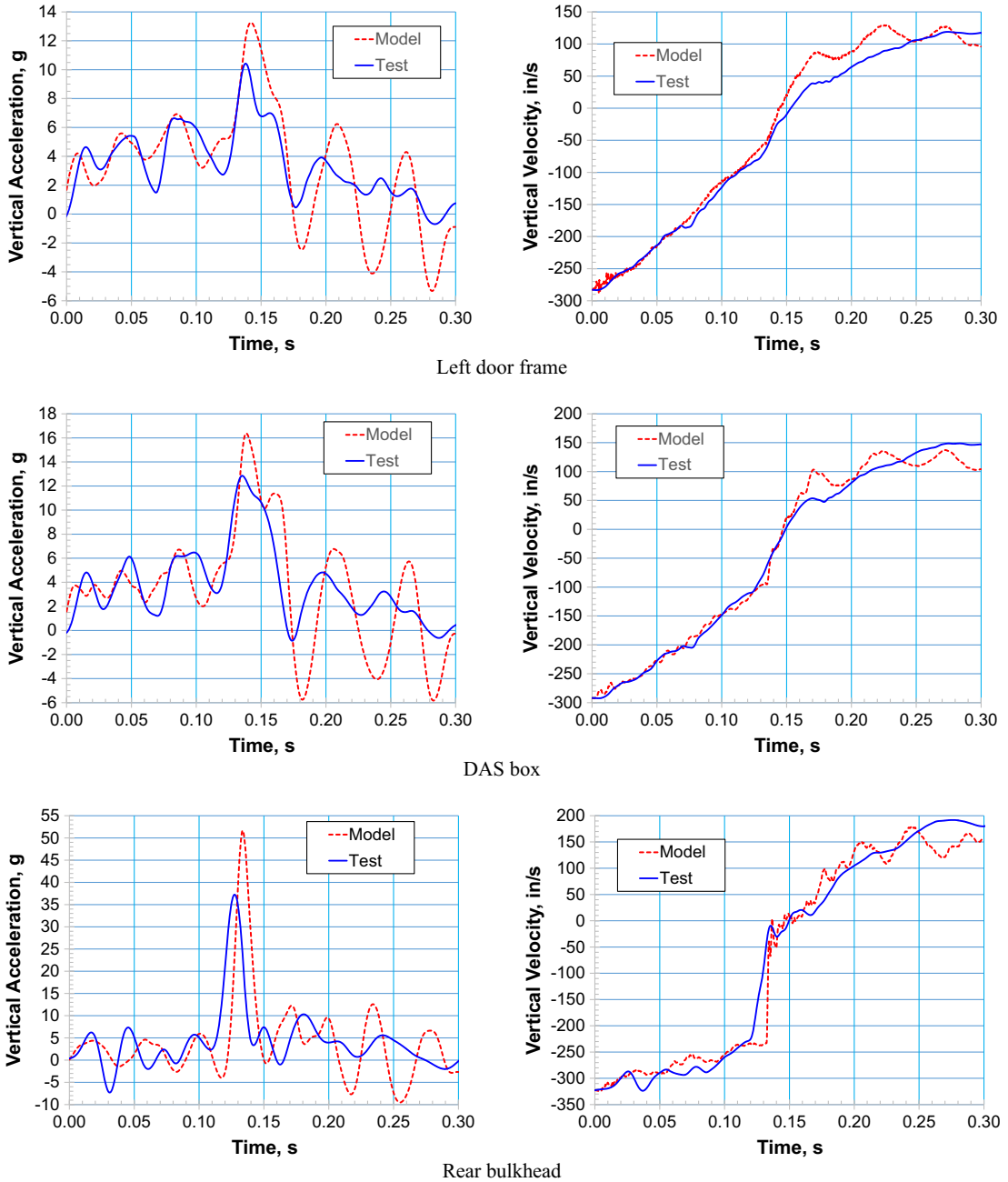

Fig. 10 Test and analysis results of local vertical acceleration and global vertical velocity in test 1.

vertical *Z* axes directions at several locations in the airframe are presented. Comparisons in the *Z*-axis direction are presented for three selected locations in the airframe (left door frame, DAS box, and rear bulkhead) in Fig. 13. Test and analytical acceleration data are filtered using an SAE CFC 20 low-pass filter and are presented in the local reference frame (moves with aircraft as shown in Fig. 3) of each accelerometer. Velocities are presented in the global coordinate system (as shown in Fig. 11).

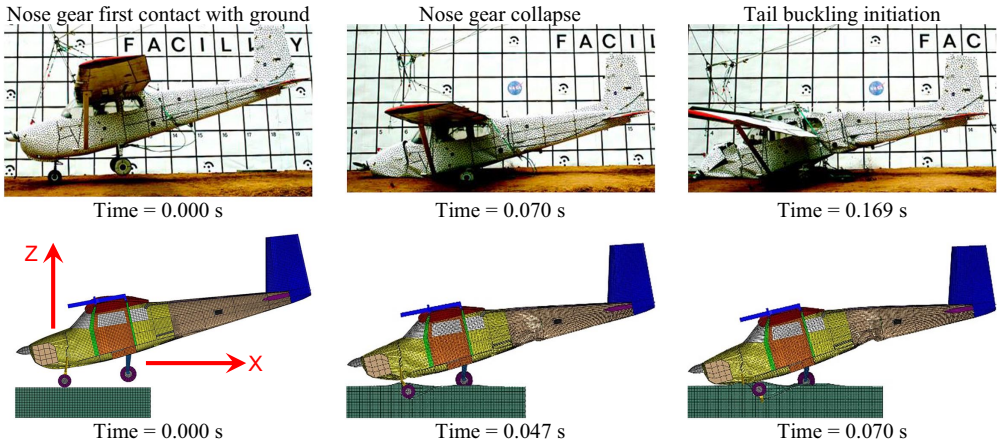

Fig. 11 Photographic images and computational models at critical kinematic events for test 2.

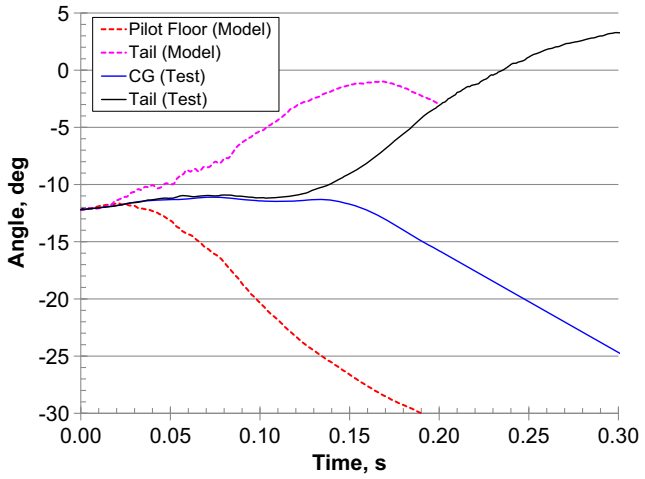

Fig. 12 Pitch angle from test and simulation against time for two locations in test 2.

Test and analysis comparisons of the delta velocity and average accelerations in the airframe shown in Table 7 are good to excellent. The test and model delta velocities were within 21% at all accelerometer locations in the airframe, with the difference between test and model data below 10% at most locations. A comparison of the peak accelerations is good in the *X* direction, but it is good to poor in the *Z* direction. The test and model peak accelerations were within 23 and 29% in the horizontal and vertical directions for all but two locations in the airframe. During the test, the left door opened, but this effect is not modeled and could contribute to the 50.6% difference in peak acceleration (which is also seen in the acceleration plot in Fig. 13). Buckling in the tail section is particularly difficult to simulate because it can be significantly affected by even small imperfections in the fuselage geometry of the tail section and by the weight distribution within the tail. These uncertainties in the geometry of the tail section are likely the major contributors to the 91.3% difference in the peak acceleration. Additionally, the Mohr–Coulomb model is a relatively simple material model and may not adequately represent the soil behavior. The simple Mohr–Coulomb model may contribute to the time difference (around 0.07 s.) in the occurrence of the acceleration and velocity peaks in Fig. 13, as described in this section of the kinematic events.

C. Crash Test 3

A sequence of photographs taken from the high-speed camera is shown in Fig. 14, along with corresponding views of the matching model kinematics. Note that the simulation model is cut in half to show the internal structure and the nose gear soil penetration. The pitch angle from photogrammetry during the test and simulation is plotted against time in Fig. 15. The test and model pitch angle time histories match closely for the first 0.05 s after impact and remain within 4 deg for the remainder of the photogrammetry data, but the tail separation angle is much more severe in the simulation. Additionally, in the simulation, the cabin section of the fuselage is not in contact with the ground at the time of tail failure as it is in the test. This delay in fuselage contact is probably due to a stiffness difference in the main landing gear, in the soil, or both. Overall, the motion of the forward fuselage in the simulation is similar to the test.

In Table 8, a comparison of the test and analysis results of the delta velocity, the average acceleration, and the peak acceleration in the *X* and *Z* axes directions at several locations in the airframe are presented. Comparisons in the *Z* axis direction are presented for three

Table 7 Comparison of test and analysis of velocity and acceleration at several locations for test 2

	Average acceleration, g			Peak acceleration, g			Delta velocity, in./s		
	Test	model	Difference, %	Test	Model	Difference, %	Test	Model	Difference, %
Pilot X	−9.2	−7.7	−16.2	−23.5	−21.7	−7.6	523.3	531.5	1.6
Copilot X	−9.3	−7.6	−17.9	−24.0	−20.8	−13.1	512.5	520.5	1.6
Left door X	−9.3	−8.1	−12.9	−21.6	−18.7	−13.5	455.4	510.4	12.1
Right door X	−6.7	−8.1	20.9	−23.5	−18.3	−22.3	421.9	511.0	21.1
DAS X	−8.8	−10.0	12.8	−33.5	−30.8	−8.1	412.9	466.5	13.0
Rear bulkhead X	−7.6	−8.1	6.0	−15.4	−16.5	6.8	325.7	354.8	8.9
Ceiling X	−7.4	−9.5	28.2	−16.5	−18.9	14.2	319.8	373.8	16.9
Pilot Z	5.2	5.4	3.3	15.9	12.9	−19.3	475.1	518.6	9.2
Copilot Z	5.0	5.8	15.6	19.2	16.2	−15.5	444.7	504.6	13.5
Left door Z	7.5	9.0	19.7	28.3	14.0	−50.6	583.4	570.2	−2.3
Right door Z	8.4	8.3	−1.6	19.1	14.1	−26.0	490.9	519.1	5.7
DAS Z	9.4	8.7	−6.9	21.1	24.4	15.5	686.1	625.3	−8.9
Rear bulkhead Z	8.5	10.9	28.0	13.0	24.8	91.3	529.9	528.5	−0.3
Ceiling Z	7.9	7.3	−7.9	24.2	17.3	−28.7	549.5	528.7	−3.8

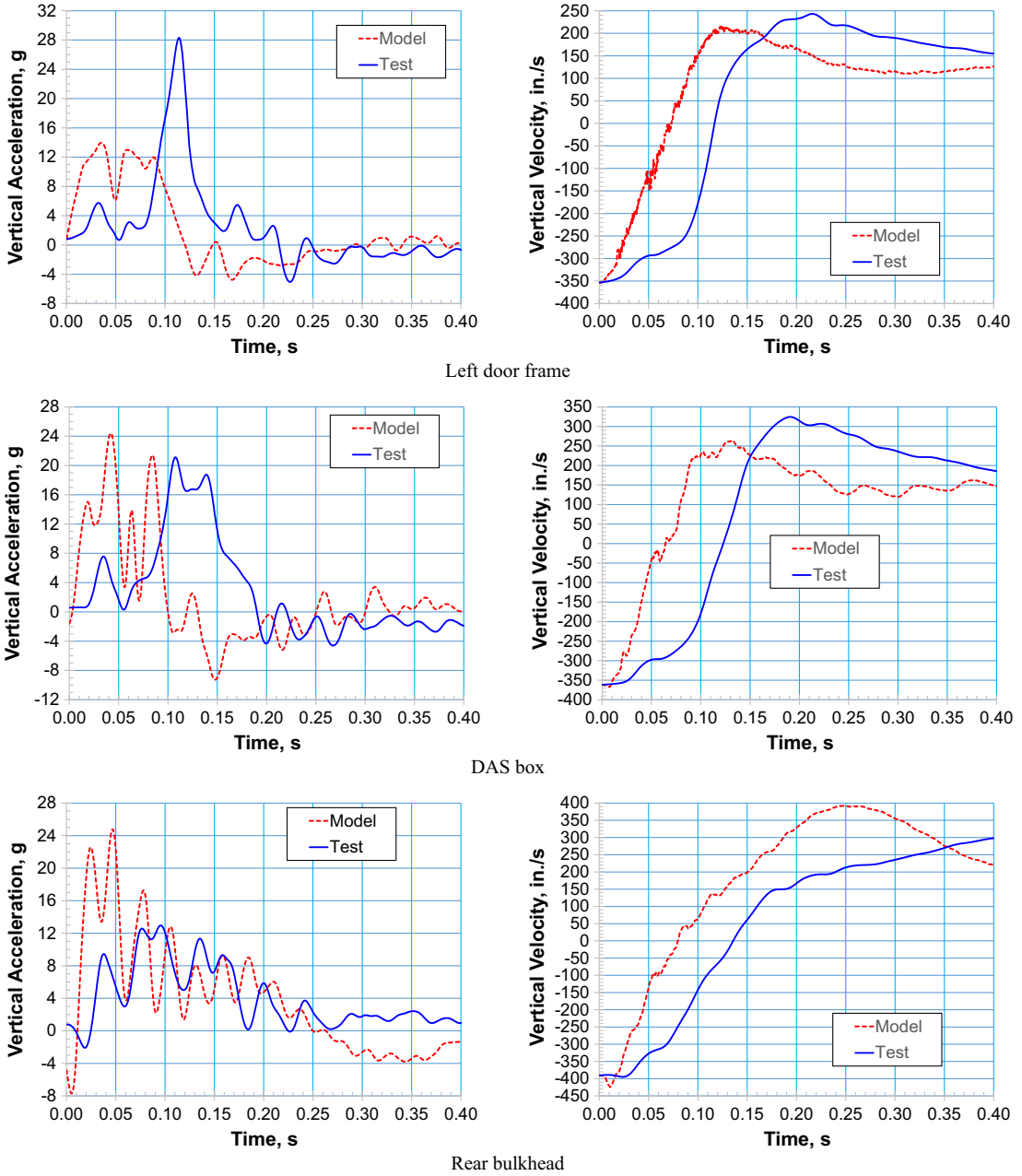

Fig. 13 Test and analysis results of local vertical acceleration and global vertical velocity in test 2.

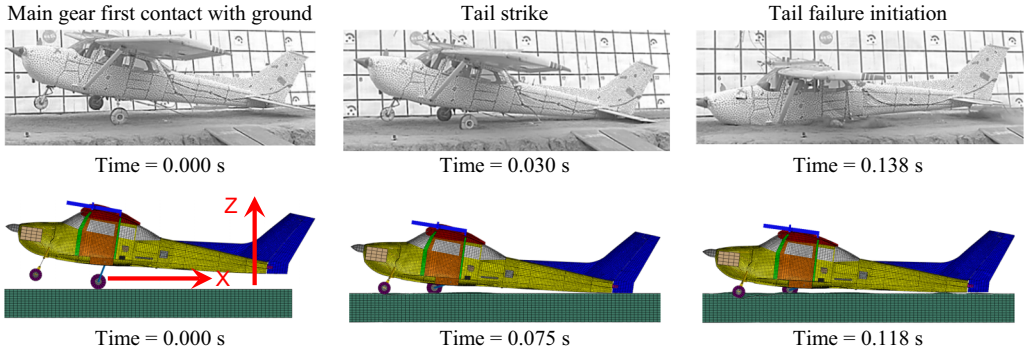

Fig. 14 Photographic images and computational models at critical kinematic events for test 3.

selected locations in the airframe (left door frame, DAS box, and rear bulkhead) in Fig. 16. Test and analytical acceleration data are filtered using an SAE CFC 20 low-pass filter and are presented in the local reference frame (moves with aircraft as shown in Fig. 4) of each accelerometer. Velocities are presented in the global coordinate system (as shown in Fig. 14).

Test and analysis comparisons of the delta velocities in the airframe shown in Table 8 are good to excellent (within 17%), except in

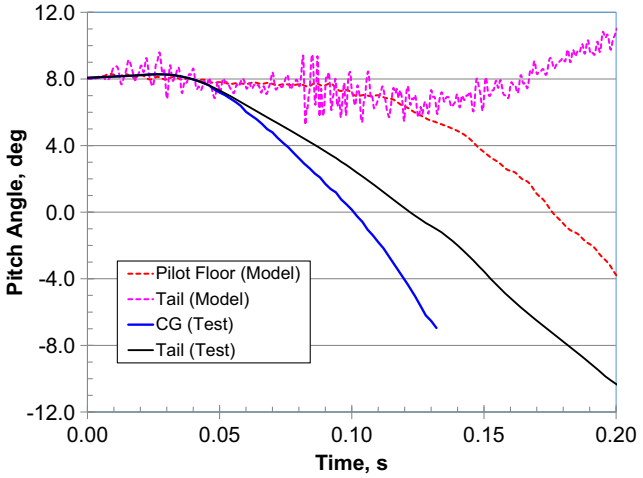

Fig. 15 Pitch angle from test and simulation against time for two locations in test 3.

the tail due to the large damage that occurs there. The poor correlation in the tail is also seen in the delta-velocity plot in Fig. 16. Correlation of the average and peak accelerations is good to excellent in the *Z* direction, except at the damaged firewall (24%). Also, note that in Fig. 16, the timing of the acceleration and velocity peaks in the *Z* direction from the simulation and the test are close (within around 0.02 s). In Table 8, correlation of the average and peak accelerations in the *X* direction is poor, probably because of the delay in the fuselage impact with the ground, as described in the previous discussion of the kinematic events. The delay in the simulation results in a reduction of the time that the belly of the fuselage is in contact with the soil, and hence a reduction in the horizontal deceleration due to friction between the fuselage and the soil. The delay could be due to uncertainty of the stiffness of the landing gear and uncertainty in the definition of the 0 deg pitch angle of the model and the test article. Additionally, the Mohr–Coulomb model is a relatively simple material model and may not adequately represent the soil behavior.

Summaries of the comparison of the test and analysis results of the vertical delta velocity and vertical acceleration at three airframe locations (left door frame, DAS box, and rear bulkhead) for all three tests are presented in Tables 9 and 10, respectively.

IV. Mesh Refinement and Parametric Studies

Results from the numerical FE models described in this paper are affected by numerous uncertainties. These uncertainties include material thicknesses in components that could not be easily measured, uncertainties in impact surface conditions, and numerical uncertainties due to effects of the finite element mesh size. In this section, a mesh convergence study is conducted and the effects of several key parameters on the numerical response of the Cessna model are described.

A. Numerical Mesh Convergence

The internal structures of all three FE models were similar. As shown in Fig. 17, the fuselage frames, wing spars, wing ribs, empennage spars, and empennage ribs were modeled with shell elements. In most components of the FE model, a minimum of three shell elements was used to properly represent the bending shape of the structure. In the fuselage frames and stringers, this minimum of three elements was used in the mesh. In the ribs and spars, four elements were used. In the wing cover panels and fuselage panels, significantly more elements were used (typically eight to 20 elements). Adequate mesh refinement was desired in regions that were critical to the deformation response of the aircraft (such as the landing gear) and regions that contained accelerometers (such as the bulkheads). A formal mesh convergence study for an entire Cessna FE model was not performed, but mesh refinements of the landing gear support and aft bulkhead (shown in Figs. 18 and 19, respectively) were performed. In the refined meshes, the element size was cut in half in both directions. Only the responses due to test 1 landing conditions were studied.

In Fig. 20, the effect of the mesh refinement on the pitch response and accelerations in the vertical coordinate system are shown. The shapes and peaks of the pitch angle responses and accelerations for the refined mesh are very close to the baseline responses. In Table 11, the maximum pitch angle and peak vertical acceleration for the refined meshes are within 1.4 and 3.5%, respectively, of the baseline values, and so the baseline mesh is considered to be converged.

B. Parametric Studies

Several types of uncertainties affect the test and numerical results in this paper. The test results are subject to uncertainties in the measurement equipment and data processing. To deal with these uncertainties, the accelerometers used in the tests are calibrated to an accuracy of 1% of reference input. No other uncertainty data are available for the test setup. The numerical models are subject to modeling uncertainties, i.e., differences between the physical test specimens and the numerical representation of those specimens. To evaluate the sensitivity of the numerical results to some of these modeling uncertainties, a series of parametric studies are conducted to evaluate the effects of three key model parameters: friction between the ground and the tires, thickness in the main landing gear strut support, and thickness of the aft bulkhead.

In Fig. 21, the sensitivity of the pitch response and accelerations in the vertical coordinate system to reduction in the ground friction and increases in the main landing gear support and rear bulkhead thicknesses are shown. When the ground friction is reduced, the landing gear tends to spread outward (in the *Y* direction) more, resulting in a

Table 8 Comparison of test and analysis of velocity and acceleration at several locations for test 3

	Average acceleration, g			Peak acceleration, g			Delta velocity, in./s		
	Test	Model	Difference, %	Test	Model	Difference, %	Test	Model	Difference, %
Pilot X	−5.8	−4.1	−30.1	−16.8	−10.9	−34.9	496.7	419.1	−15.6
Copilot X	−6.3	−4.0	−36.6	−16.6	−10.7	−35.6	504.0	418.7	−16.9
Left door X	−5.3	−3.6	−31.4	−14.9	−10.9	−27.0	467.4	390.1	−16.5
Right door X	−5.5	−3.8	−30.3	−13.9	−11.1	−20.0	437.8	390.9	−10.7
DAS X	−5.2	−3.4	−33.2	−14.1	−12.1	−13.9	365.5	363.0	−0.7
Rear bulkhead X	−4.4	−3.4	−22.9	−11.5	−12.0	5.0	319.7	348.3	8.9
Ceiling X	−4.0	−2.1	−48.4	−9.4	−7.7	−17.9	255.3	234.6	−8.1
Firewall X	−6.5	−3.5	−45.7	−22.0	−9.6	−56.5	284.2	295.2	3.9
Pilot Z	6.0	5.2	−13.0	16.6	13.5	−18.3	572.0	483.5	−15.5
Copilot Z	5.7	4.8	−16.3	15.7	14.1	−10.1	527.7	483.5	−8.4
Left door Z	7.6	6.5	−14.5	17.5	16.8	−4.1	664.5	570.2	−14.2
Right door Z	6.8	6.6	−4.0	20.2	16.4	−18.6	664.2	569.5	−14.3
DAS Z	8.1	7.1	−12.4	26.8	25.0	−6.6	723.7	690.3	−4.6
Rear bulkhead Z	9.2	7.4	−19.7	32.5	31.4	−3.4	842.2	574.9	−31.7
Ceiling Z	6.3	6.3	0.8	19.8	21.0	6.2	598.1	555.3	−7.2
Firewall Z	6.6	5.0	−23.8	14.2	12.3	−13.5	357.9	335.2	−6.3

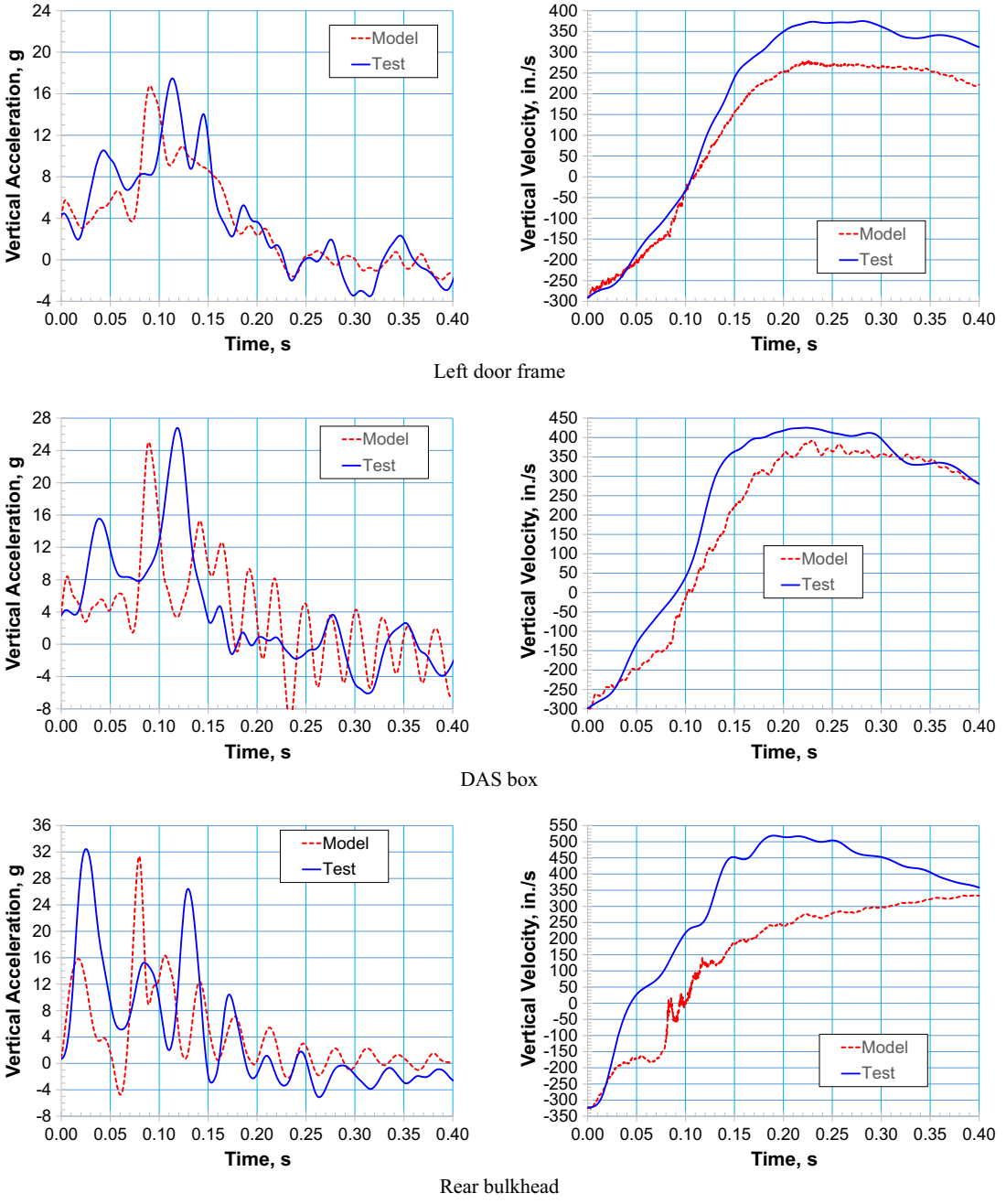

Fig. 16 Test and analysis results of local vertical acceleration and global vertical velocity in test 3.

Table 9 Test and analysis comparisons of vertical delta velocity

	Difference, %		
Location	Test 1	Test 2	Test 3
Left door frame	2.1	−2.3	−14.2
DAS box	−2.6	−8.9	−4.6
Rear bulkhead	−2.2	−0.3	−31.7

Table 10 Test and analysis comparisons of peak vertical acceleration

	Difference, %		
Parameter	Test 2	Test 2	Test 3
Left door frame	27.4	−50.6	−4.1
DAS box	27.4	15.5	−6.6
Rear bulkhead	38.7	91.3	−3.4

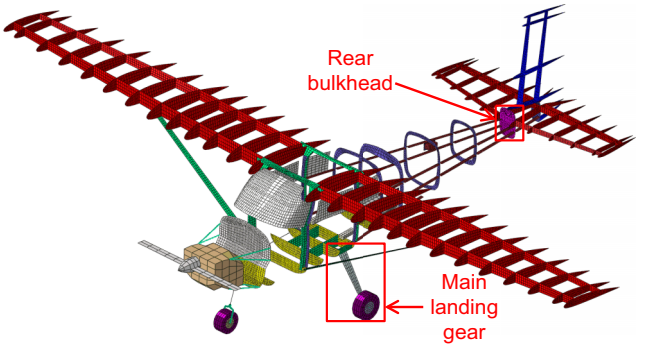

Fig. 17 Internal structure of the FE model of the C-172 airframe (tests 1 and 2).

slightly lower maximum pitch angle and an increase in accelerations at the pilot floor and in the tail section. A 10% increase in the thickness of the support structure for the landing gear has the opposite

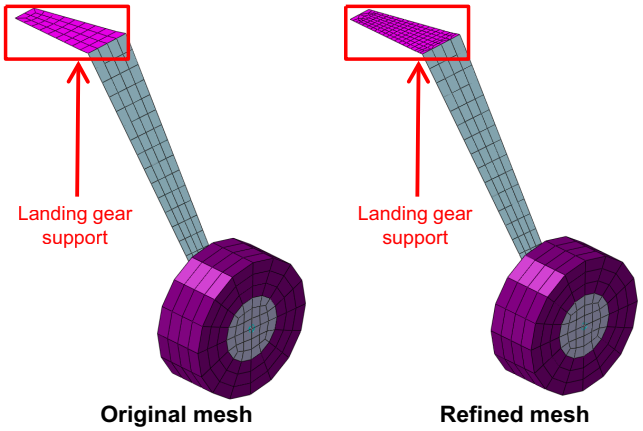

Fig. 18 Mesh refinement of landing gear support component.

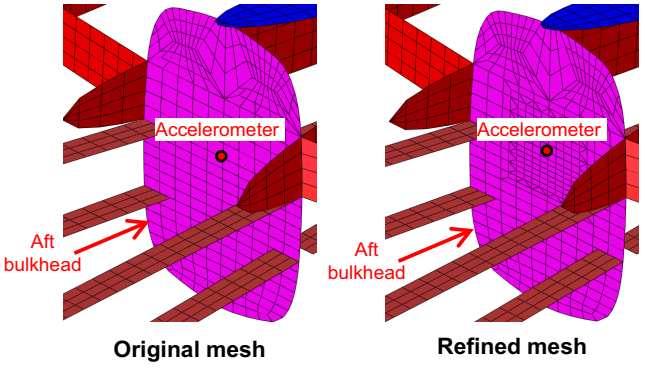

Fig. 19 Mesh refinement of aft bulkhead component.

Table 11 Comparison of pitch response and accelerations of baseline and refined meshes

Parameter	Difference for refined support mesh, %	Difference for refined bulkhead mesh, %
Pitch angle at pilot floor	1.2	−0.3
Pitch angle at tail	1.4	0.9
Acceleration at left door frame	0.2	−2.9
Acceleration at rear bulkhead	3.5	−0.2

effect, making the landing gear a stiffer spring, delaying the rebound response of the vehicle, and significantly reducing the accelerations. A 20% increase in the thickness of the rear bulkhead reduces the pitch angle response by less than 2% and reduces the accelerations by less than 4%. According to Table 12, the increase in the thickness of the landing gear support structure has the greatest effect on the structural response, with a 10% increase in pitch angle and a 28.6% decrease in accelerations in the tail section.

V. Conclusions

Test data from three full-scale aircraft impact tests and corresponding computer simulations analyzed using the Abaqus explicit FE software are presented in this paper. An advanced modeling tool was used to generate a complete FE model from a combination of planform dimensions and a series of manual measurements of the test aircraft. The predictive model required only minor calibration once the test data were captured. The calibrated model was obtained by making small adjustments to the nonstructural masses and modifying

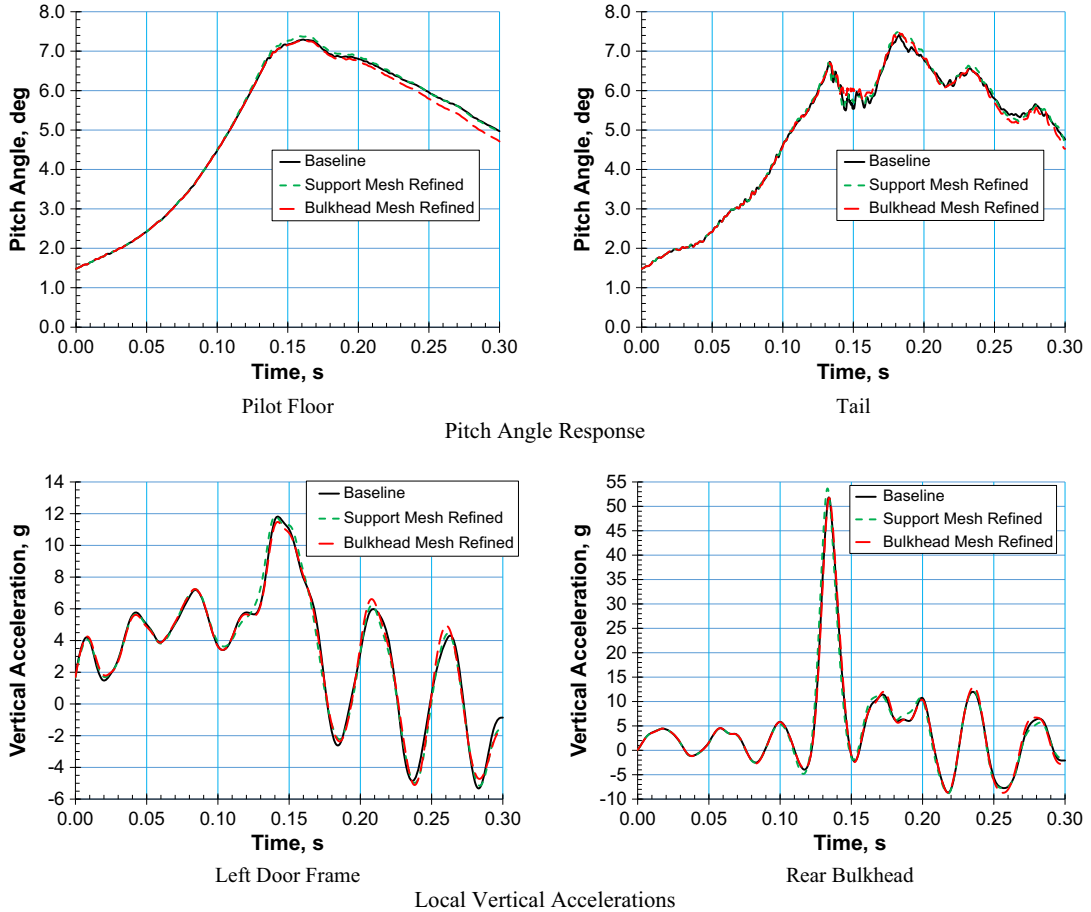

Fig. 20 Sensitivity of pitch angle response and local vertical acceleration due to mesh refinement.

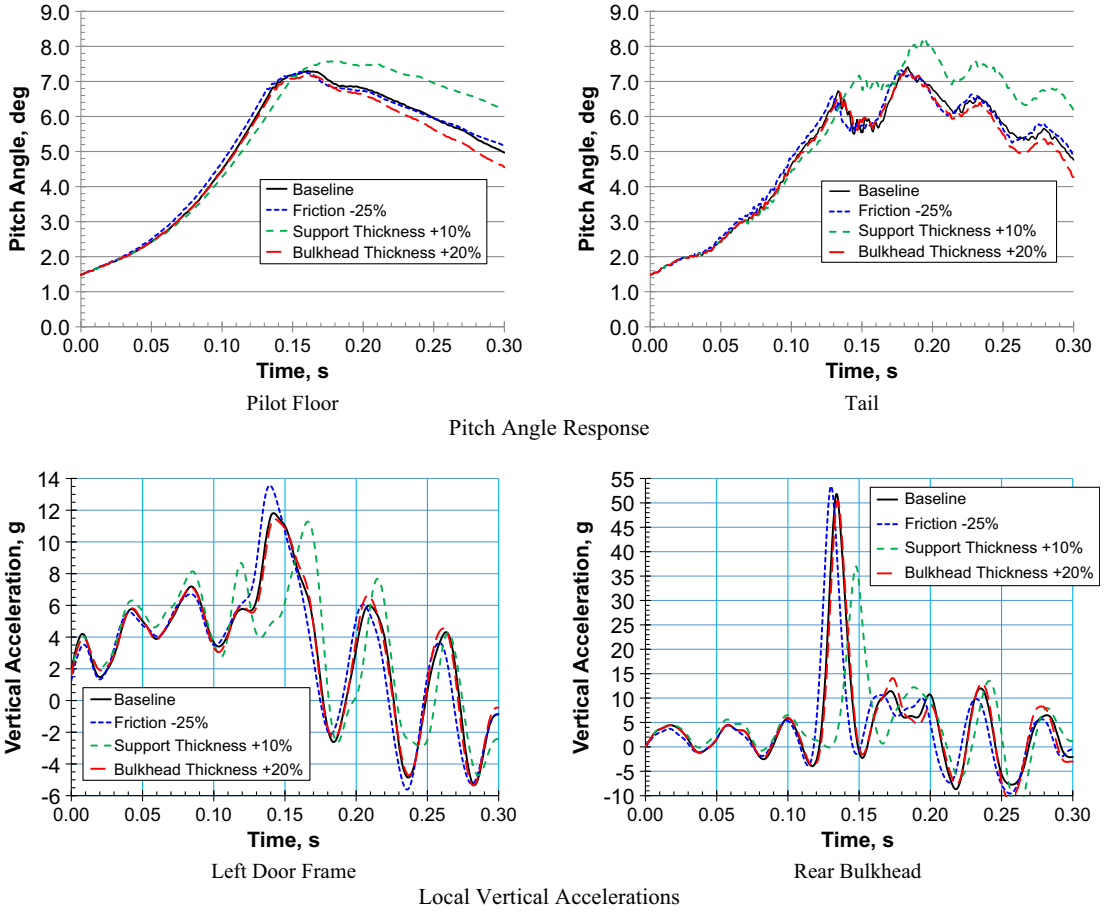

Fig. 21 Sensitivity of pitch angle response and local vertical acceleration to changes in friction and thickness.

Table 12 Sensitivity of pitch response and accelerations to friction and thickness changes

Parameter	Change due to decrease in friction, %	Change due to increase in support thickness, %	Change due to increase in bulkhead thickness, %
Pitch angle at pilot floor	−0.3	3.9	−1.6
Pitch angle at tail	−1.2	10.0	−0.9
Acceleration at left door frame	14.7	−4.6	−3.2
Acceleration at rear bulkhead	3.0	−28.6	−2.6

the landing gear stiffnesses to match the physical properties of the actual test aircraft.

Comparisons of the test and analysis data included inertial properties, time histories of the airframe motion (pitch angle), and time histories of the velocities and accelerations. The overall findings of the study are as follows:

1) The total weight of the models matched the test articles within 0.001%, and the CG locations matched within 0.4%, which are considered in excellent agreement.

2) The kinematic responses of the model were similar to the tests, although a time shift in the response was noted, probably due to uncertainties in the soil properties.

3) The delta velocities of the model and test were within 10% for the majority of the airframe locations in all tests.

4) The peak accelerations for the model were usually within 20 to 40% of the values for the test, except at the tail and firewall, which were damaged in tests 2 and 3.

5) Uncertainties in the weight distribution, unmodeled components, and soil properties contributed to most of the discrepancies between test and analysis.

6) Damage to the aircraft fuselage occurred immediately aft of the cabin section in all three crash scenarios; consequently, the wires connecting the ELT to the antenna should not cross this axial position in the aircraft. Installation of the ELT and its antenna in close proximity to each other minimizes the risk that the connecting wires are routed through an area that can experience severe damage, thus compromising the connection.

7) Mounting an ELT in a location subject to very large accelerations at lower impact velocities (such as the rear bulkhead) should be avoided to prevent activation of the ELT during minor incidents, such as a runway bump.

8) Mesh refinement resulted in a small (3.5%) change in peak accelerations, and so the model was considered to be converged.

9) A parameter study was used to demonstrate that the response of the aircraft model is very sensitive to the thickness of the landing gear support structure (with a 28.6% increase in peak acceleration from a 10% change in thickness) and is much less sensitive to the thickness of the aft bulkhead and soil friction.

Due to the excellent correlation between the analysis and test, the simulation models are suitable for further studies evaluating alternative ELT mounting configurations and for evaluating airframe performance under different impact conditions.

Acknowledgments

The authors of this paper are employed by the National Aeronautics and Space Administration (NASA), and the research presented in this paper was directly funded by the U. S. Government. The use of trademarks or names of manufacturers in this paper is for accurate reporting and does not constitute an official endorsement, either expressed or implied, of such products or manufacturers by NASA.

References

[1] "Installation and Inspection Procedures for Emergency Locator Transmitters and Receivers," U.S. Dept. of Transportation, Federal Aviation Administration Advisory Circular 91-44A, Feb. 2018, https://www.faa.gov/documentLibrary/media/Advisory_Circular/AC_91-44A_CHG-1.pdf.

[2] "NASA's Gantry: Past, Present and Future Asset to Exploration." NASA Fact Sheet FS-2007-08-138-LaRC, http://www.nasa.gov/centers/langley/news/factsheets/fs-2007-08-138-larc.html [retrieved 11 Jan. 2023].

[3] Vaughan, V. L., Jr., and Alfaro-Bou, E., "Impact Dynamics Research Facility for Full-Scale Aircraft Crash Testing," NASA TN-D-8179, April 1976.

[4] Littell, J. D., "Crash Tests of Three Cessna 172 Aircraft at NASA Langley Research Center's Landing and Impact Research Facility," NASA TM-2015-218987, Nov. 2015.

[5] Castle, C. B., and Alfaro-Bou, E., "Light Airplane Crash Tests at Three Flight-Path Angles," NASA TP-1210, June 1978.

[6] Hayduk, R. J., "Comparative Analysis of PA-31-350 Chieftain (N44LV) Accident and NASA Crash Test Data," NASA TM-80102, Oct. 1979.

[7] Castle, C. B., and Alfaro-Bou, E., "Light Airplane Crash Tests at Three Roll Angles," NASA TP-1477, Oct. 1979.

[8] Vaughan, V. L., Jr., and Alfaro-Bou, E., "Light Airplane Crash Tests at Three Pitch Angles," NASA TP-1481, Nov. 1979.

[9] Vaughan, V. L., Jr., and Hayduk, R. J., "Crash Tests of Four Identical High-Wing Single Engine Airplanes," NASA TP-1699, Aug. 1980.

[10] Alfaro-Bou, E., Williams, M. S., and Fasanella, E. L., "Determination of Crash Test Pulses and Their Application to Aircraft Seat Analysis," SAE International TP 810611, Warrendale, PA, 1981. https://doi.org/10.4271/810611

[11] Williams, M. S., and Fasanella, E. L., "Crash Tests of Four Low-Wing Twin-Engine Airplanes with Truss-Reinforced Fuselage Structure," NASA TP-2070, Sept. 1982.

[12] Carden, H. C., "Correlation and Assessment of Structural Airplane Crash Data with Flight Parameters at Impact," NASA TP-2083, Nov. 1982.

[13] Melosh, R. J., and Kamat, M. P., "Computer Simulation of Light Aircraft Crash," *Journal of Aircraft*, Vol. 14, No. 10, Oct. 1977, pp. 1009–1014. https://doi.org/10.2514/3.44631

[14] "Emergency Landing Dynamic Conditions," *Airworthiness Standards: Normal, Utility, Acrobatic, and Commuter Category Airplanes*, Pt. 23, Title 14: Aeronautics and Space, Federal Aviation Administration, U.S. Dept. of Transportation Code of Federal Regulations 23.562, Jan. 2011.

[15] Jackson, K. E., Boitnott, R. L., Fasanella, E. L., Jones, L. E., and Lyle, K. H., "A History of Full-Scale Aircraft and Rotorcraft Crash Testing and Simulation at NASA Langley Research Center," NASA TM-2004-0191337, Jan. 2004.

[16] Hurley, T. R., and Vandenburg, J. M., (eds.), "Small Airplane Crashworthiness Design Guide," Simula Technologies TR-98099, Phoenix, AZ, April 2002; also NASA, AGATE Integrated Design and Manufacturing Technical Council Rept. AGATE-WP3.4-034043-036, April 2002.

[17] Jackson, K. E., and Fasanella, E. L., "NASA Langley Research Center Impact Dynamics Research Facility Research Survey," *Journal of Aircraft*, Vol. 41, No. 3, May 2004, pp. 511–522. https://doi.org/10.2514/1.3082

[18] Thomson, R. G., and Goetz, R. C., "NASA/FAA General Aviation Crash Program—A Status Report," *Journal of Aircraft*, Vol. 17, No. 8, Aug. 1980, pp. 584–590. https://doi.org/10.2514/3.57943

[19] Wittlin, G., "Analysis of Aircraft Dynamic Behavior in a Crash Environment," *Journal of Aircraft*, Vol. 20, No. 9, Sept. 1983, pp. 762–769. https://doi.org/10.2514/3.44940

[20] McComb, H. G., Jr., Thomson, R. G., and Hayduk, R. J., "Structural Dynamics Research in a Full-Scale Transport Aircraft Crash Test," *Journal of Aircraft*, Vol. 24, No. 7, July 1987, pp. 447–453. https://doi.org/10.2514/3.45500

[21] Thomas, M., Chitty, D., Gildea, M., and T'Kindt, C., "Constitutive Soil Properties for Unwashed Sand and Kennedy Space Center," NASA CR-2008-215334, July 2008.

[22] Annett, M. S., Little, J. D., Jackson, K. E., Bark, L. W., DeWeese, R. L., and McEntire, B. J., "Evaluation of the First Transport Rotorcraft Airframe Crash Testbed (TRACT 1) Full-Scale Crash Test," NASA TM-2014-218543, Oct. 2014.

[23] Annett, M. A., Littell, J. D., Stimson, C. M., Jackson, K. E., and Mason, B. H., "Full-Scale Crash Tests and Analyses of Three High-Wing Single Engine Aircraft," *Aerospace Structural Impact Dynamics International Conference*, ASIDIC, Nov. 2015.

[24] Jackson, K. E., and Fasanella, E. L., "Crash Testing and Simulation of a Cessna 172 Aircraft: Hard Landing onto Concrete," *14th International LS-DYNA Users Conference*, Livermore Software Technology Corp., June 2016.

[25] Fasanella, E. L., and Jackson, K. E., "Crash Testing and Simulation of a Cessna 172 Aircraft: Pitch Down Impact onto Soft Soil," *14th International LS-DYNA Users Conference*, Livermore Software Technology Corp., June 2016.

[26] Mason, B. H., and Quinlan, J. R., "Conceptual Design Shop: A Tool for Rapid Airframe Structural Modeling," *59th AIAA/ASCE/AHS/ASC SDM Conference*, AIAA Paper 2018-2001, Jan. 2018. https://doi.org/10.2514/6.2018-2001

[27] *PATRAN Software Package*, Ver. 2016, MSC Software, Santa Ana, CA, 2016.

[28] *Abaqus Software Package*, Ver. 6.14, Dassault Systèmes Simulia Corp., Pawtucket, RI, 2012.

[29] "Recommended Practices: Instrumentation for Impact Test—Part 1—Electronic Instrumentation," *SAE International Standard* J211-1, Warrendale, PA, March 1995.